On the dominance of trivial knots among SAPs on a cubic lattice

2001 J. Phys. A: Math. Gen. 34 7563

(http://iopscience.iop.org/0305-4470/34/37/310)

INSTITUTE OF PHYSICS PUBLISHING JOURNAL OF PHYSICS A: MATHEMATICAL AND GENERAL

J. Phys. A: Math. Gen. **34** (2001) 7563–7577 PII: S0305-4470(01)22418-4

On the dominance of trivial knots among SAPs on a cubic lattice

Akihisa Yao[1], Hiroshi Matsuda[1], Hiroshi Tsukahara[2], Miyuki K Shimamura[3] and Tetsuo Deguchi[4]

[1] Department of Physics, Faculty of Science and Engineering, Chuo University, 1-13-27 Kasuga, Bunkyo-ku, Tokyo 112-8551, Japan
[2] Geographic Information Systems Department, Hitachi Software Engineering Co. Ltd, Kita-3, Nishi-3, Chuo-ku, Sapporo 060-0003, Japan
[3] Graduate School of Frontier Sciences, University of Tokyo, 7-3-1 Hongo, Bunkyo-ku, Tokyo 113-8656, Japan
[4] Department of Physics, Faculty of Science and Graduate School of Humanities and Sciences, Ochanomizu University, 2-1-1 Ohtsuka, Bunkyo-ku, Tokyo 112-8610, Japan

Received 1 March 2001, in final form 19 July 2001
Published 7 September 2001
Online at stacks.iop.org/JPhysA/34/7563

Abstract

The knotting probability is defined by the probability with which an N-step self-avoiding polygon (SAP) with a fixed type of knot appears in the configuration space. We evaluate these probabilities for some knot types on a simple cubic lattice. For the trivial knot, we find that the knotting probability decays much slower for the SAP on the cubic lattice than for continuum models of the SAP as a function of N. In particular the characteristic length of the trivial knot that corresponds to a 'half-life' of the knotting probability is estimated to be 2.5×10^5 on the cubic lattice.

PACS numbers: 05.50.+q, 02.10.Kn

1. Introduction

The self-avoiding polygon (SAP) with fixed topology gives a simplified model of real ring polymers in solution that have a topological constraint as well as excluded volume. Throughout the time evolution, a circular polymer keeps the same knot which is given to it when it is made; it does not change its topology under any thermal fluctuations since no crossing through itself is allowed. On the other hand, the SAP corresponds to the special case of the self-avoiding walk (SAW) that returns to the origin. If we construct a set of SAPs, then their topological states may contain several different knots. Therefore, it is not trivial how to realize the topological constraint on a SAP. One possible method for assigning the topological constraint on a SAP is that after generating a large number of SAPs we select only such SAPs that have the same given knot. By this method, we can assign the topological constraint on any SAP model. In

this context, the probability that a given SAP has a fixed knot plays a central role, and we call it the *knotting probability* of the SAP model for the knot. Among many different models, the SAP on the cubic lattice with fixed topology is one of the most fundamental SAP models. It has an advantage that the definition is very simple. We expect that the model should be suitable for general and mathematical study. In fact, several rigorous results on knotting probability have been derived for the SAP on the cubic lattice [1–4]. Thus, the main motivation behind the present research is to characterize the knotting probability of the SAP on the cubic lattice through numerical simulations.

Let us discuss some previous numerical results on SAP knotting probabilities [5–16]. For a SAP model (or random polygon) with N steps, we denote by $P_{\mathrm{K}}(N)$ the knotting probability of the model for knot K. For the Gaussian model of random polygon and the rod–bead SAP model, knotting probabilities were evaluated through numerical simulations for the trivial knot $K = \emptyset$ [6, 8, 10] and also for some non-trivial knots [5, 12–15]. It was found that for the SAP and random polygon models, the knotting probability as a function of the step number N is given by the following:

$$P_{\mathrm{K}}(N) = C(K)N^{m(K)} \exp[-N/N(K)] \tag{1.1}$$

where $C(K)$, $m(K)$ and $N(K)$ are fitting parameters. For large N, the formula (1.1) is consistent with the asymptotic expansion of the partition function of the SAP with fixed-knot type. For finite N, although it is not rigorous, it seems that the formula (1.1) fits numerical data well. From the numerical result it was conjectured that the parameter $N(K)$, which we call the characteristic length of knot K, should be given by the same value for any knot K [12]. Furthermore, it was also conjectured that the parameter $m(K)$, which we call the exponent of knot K, should be universal for different SAP or random polygon models [13–15]. We note that the fitting formula (1.1) together with the two conjectures are consistent with the standard asymptotic behaviour expected for the SAP or random polygon. Here we also note that the rod–bead model is an off-lattice SAP model.

Recently, the SAP on the cubic lattice with a fixed knot was studied through a numerical simulation using the BFACF algorithm, which generates SAPs with the same fixed knot but different step numbers N [16]. In the simulation, the exponent $m(K)$ and the growth constant for the number of allowed configurations of the SAP with knot K has been estimated for some knots. Furthermore, it was shown that the knotting probability for the trivial knot decays 'exponentially' for a face-centred cubic (FCC) lattice [11] and for the cubic lattice [3]. However, any precise estimate of the knotting probability or the characteristic length $N(K)$ has not been given for the cubic lattice. Thus, it is the primary purpose of this paper to evaluate the characteristic length $N(K)$ for the SAP on the cubic lattice.

In 1962, Delbrück [17] noticed that the topological constraint may be very important for polymers in biology and chemistry. Since then, the topological problem has been studied in several approaches in physics and mathematics. As one of the earliest studies, des Cloizeaux and Mehta [18] estimated through numerical simulations the critical exponent ν for the internal distance of the Gaussian random polygon and discussed some possible properties of random polygons under the topological constraint.

After the rediscovery of the pivot algorithm, many SAW and SAP properties have been investigated not only in field theory but also by computer simulations [20, 21]. It seems, however, that there are only a few works such as [16, 19] where the gyration radius $\langle R_{\mathrm{G}}^2 \rangle_{\mathrm{SAP}}$ of the SAP on the cubic lattice is studied by numerical simulations. Let us denote by $\langle R_{\mathrm{G}}^2 \rangle_{\mathrm{SAW}}$ and $\langle R_{\mathrm{G}}^2 \rangle_{\mathrm{SAP}}$ the mean square of the gyration radius of the SAW and SAP, respectively. It is interesting to evaluate the universal amplitude ratio between $\langle R_{\mathrm{G}}^2 \rangle_{\mathrm{SAP}}$ and $\langle R_{\mathrm{G}}^2 \rangle_{\mathrm{SAW}}$. The ratio has been evaluated only up to $O(\varepsilon)$ in the ε-expansion method [22]. Furthermore, according

to the scaling theory of polymers, the exponent ν_{SAP} for $\langle R_{\mathrm{G}}^2\rangle_{\mathrm{SAP}}$ should be given by the exponent ν_{SAW} for $\langle R_{\mathrm{G}}^2\rangle_{\mathrm{SAW}}$. The agreement is confirmed up to $O(\varepsilon)$ by renormalization group theory [22, 23]. However, it is nontrivial to confirm the agreement for the SAP on the cubic lattice through numerical simulations. Thus, the numerical study of the gyration radius for the SAP on the cubic lattice is another purpose of this research.

Hereafter in this introduction, we explain some of the main results of our numerical simulations. Employing the pivot algorithm, we construct a large number of SAPs for the SAP on the cubic lattice with given step number N. For the gyration radius, we have obtained the exponent $\nu_{\mathrm{SAP}} = 0.5867 \pm 0.0017$. This is indeed in good agreement with the estimate of the critical exponent of the SAW in the ε-expansion $\nu_{\mathrm{SAW}} = 0.5882 \pm 0.0011$. Thus, our simulation in this paper also confirms the agreement of the two exponents.

Let us explicitly consider the method for the topological constraint on the SAP in the cubic lattice with given step number N. The pivot algorithm of the SAP can generate all the allowed configurations of the SAP with equal probability. Therefore, the set of SAPs generated by the algorithm may contain various knots. Suppose that we have constructed M SAPs of step number N. Calculating some knot invariants for each of the SAPs, we effectively detect the knot types of the SAPs. We enumerate the number of such SAPs that have the same set of values of the knot invariants for knot K, and denote it by $M(K)$. The expectation value of a physical quantity under the topological constraint with fixed knot K can be effectively calculated by taking the statistical average of the quantity for the $M(K)$ SAPs.

We now turn to the knotting probability. Let the symbol $P_{\mathrm{K}}(N)$ denote the knotting probability of the SAP with N steps on the cubic lattice for knot K. If there are $M(K)$ SAPs in the total M SAPs, then we evaluate it by $P_{\mathrm{K}}(N) = M(K)/M$. In our simulation, 10^5 SAPs ($M = 10^5$) are constructed for six different values of the step number from $N = 500$ to 3000. We have found that almost all SAPs are topologically equivalent to the trivial knot, and also that the resulting values of the knotting probability for the trivial knot are fitted well by the formula (1.1). Thus, for the trivial knot, we have obtained an estimate of the characteristic length

$$N(\emptyset) = (2.5 \pm 0.3) \times 10^5. \tag{1.2}$$

This result means that trivial knots are dominant among SAPs on the cubic lattice when the step number N is less than 10^5. It implies that when $N > N(\emptyset)$, the majority of SAPs on the cubic lattice have some non-trivial knots. The large value of the characteristic length might be a consequence of the strong self-avoiding effect of the SAP on the cubic lattice.

This paper is organized as follows. In section 2 we will estimate the universal amplitude ratio and the critical exponent ν_{SAP} of the gyration radius. In section 3 we will explicitly discuss the knotting probability for the trivial knot, and obtain the estimate of the characteristic length. We will also show that the knotting probability for the trivial knot decays almost linearly since the characteristic length of the trivial knot is so large. Finally, in the last section, we will discuss the possibility that the characteristic lengths take an unique value without depending on knot types.

2. The mean-square of the gyration radius

2.1. Previous results on SAW and SAP

An N-step SAW w in $\mathbb{Z}^3$ is a sequence $w_0, w_1, \ldots, w_N$ of $N+1$ distinct points in $\mathbb{Z}^3$ such that each point w_i is one of the nearest neighbours of its predecessor w_{i-1}: $|w_i - w_{i-1}| = 1$ for $i = 1, \ldots, N$. It is also subject to a constraint that any site can never be occupied by two or

more points in a sequence $\{w_i\}$. The points w_0 and w_N are the endpoints of w. The components of w_i are represented by $w_i^{(\alpha)}$ for $\alpha = 1, 2, 3$. The SAP is a special case of the SAW that makes a ring. We consider an $(N-1)$-step SAW and denote it by $w = \{w_0, w_1, \ldots, w_{N-1}\}$. If the endpoint w_0 is the nearest neighbour of the endpoint w_{N-1}, this is an N-step SAP in $\mathbb{Z}^3$.

The mean-square of the gyration radius of the SAP $\langle R_G^2 \rangle_{SAP}$ is smaller than that of the SAW $\langle R_G^2 \rangle_{SAW}$. This fact comes from the following difference. The endpoints of the SAW are free, while those of the SAP are constrained, that is, the endpoints of the SAP should meet at the nearest neighbour sites of the lattice. This means that the SAW has a possibility of a longest end-to-end distance whereas the SAPs does not.

The RG argument gives several results for the SAW and the SAP. Among these, we are most interested in the amplitude ratio $\langle R_G^2 \rangle_{SAP} / \langle R_G^2 \rangle_{SAW}$. According to the RG theory, the amplitude ratio should be universal, i.e. it does not depend on the details of the models for the SAW or the SAP. The ratio has been evaluated by using the RG equation and the cluster expansion up to $O(\varepsilon)$ [22, 23]:

$$\frac{\langle R_G^2 \rangle_{SAP}}{\langle R_G^2 \rangle_{SAW}} = 0.568. \tag{2.1}$$

The ratio has also been estimated in [19] through numerical simulations with $N \leqslant 800$: it is given by 0.538 ± 0.006.

Another interesting result of the RG argument is that the critical exponent for the mean-square of the gyration radius is universal. It is well known that the exponent ν_{SAW} of the SAW corresponds to the critical exponent of the O(n) vector model in the limit of n going to zero. The precise estimate of the critical exponent ν_{SAW} has been made using the ε-expansion method through this correspondence [24–27]:

$$\nu_{SAW} = 0.5882 \pm 0.0011. \tag{2.2}$$

The exponent ν_{SAW} has also been precisely evaluated by Monte Carlo simulations, where the best estimate is given by the following [20]:

$$\nu_{SAW} = 0.5877 \pm 0.0006. \tag{2.3}$$

2.2. The amplitude ratio

In our simulation of SAPs on the cubic lattice, we have employed a length-conserving dynamical algorithm which keeps endpoints fixed. This algorithm was investigated in detail by Madras *et al* [20, 21]. We call this algorithm the MOS pivot for short. Some details are described in appendix A.

We calculate the ratio $\langle R_G^2 \rangle_{SAP} / \langle R_G^2 \rangle_{SAW}$ and the exponent ν_{SAP} using the MOS pivot and compare resulting values with theoretical and other simulated values. The mean square of the gyration radius is calculated using

$$\langle R_G^2 \rangle_{SAP} = \frac{1}{T} \sum_{t=1}^{T} \left[\frac{1}{N} \sum_{i=0}^{N} \left(w_i^{[t]} - \frac{1}{N} \sum_{j=0}^{N} w_j^{[t]} \right)^2 \right] \tag{2.4}$$

where T is the number of polygons and N the step number, and the symbol $w_i^{[t]}$ denotes the ith site in the tth SAP in the sequence of SAPs given by '200 successful MOS pivot operations' (see appendix A for details).

Let us note that the gyration radius should have the asymptotic behaviour

$$\langle R_G^2 \rangle_{SAP} = A_{SAP} N^{2\nu_{SAP}} (1 + B N^{-\Delta}) \qquad \text{as} \quad N \to \infty. \tag{2.5}$$

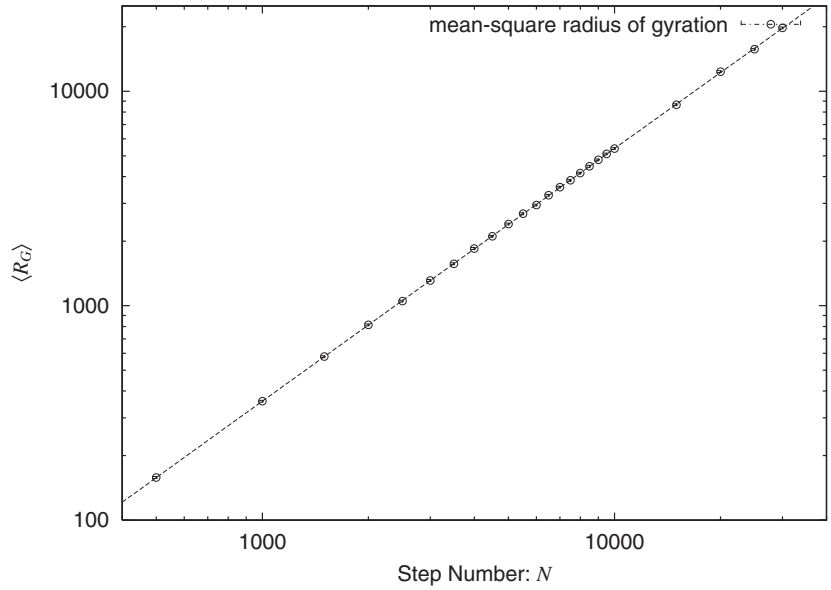

Figure 1. Mean-square radius of gyration $\langle R_{\rm G} \rangle$. We give the log–log plot of the mean square of the gyration radius versus the step number N. Here error bars denote one standard deviation.

Choosing $\frac{1}{2}$ for the exponent Δ of the correction term, the numerical data given by the equation (2.4) are plotted in figure 1 and fitted to $A_{\rm SAP} N^{2\nu_{\rm SAP}}(1 + BN^{-\frac{1}{2}})$, where $A_{\rm SAP}$, B and $\nu_{\rm SAP}$ are fitting parameters. Since there are not enough data to fit in a four-parameter curve in our simulation, we have assumed the fixed value for the exponent Δ. We plot the mean-square of the gyration radius from $N = 500$ to 30 000 in figure 1. Here, we set T, the number of polygons, to 10 000. The error bars denote one standard deviation given by the Poisson distribution to the number T of polygons with N.

The three parameters are obtained by fitting the data in figure 1:

$$\nu_{\rm SAP} = 0.5867 \pm 0.0017 \tag{2.6}$$

$$A_{\rm SAP} = 0.1101 \pm 0.0037 \tag{2.7}$$

$$B = -0.06 \pm 0.04. \tag{2.8}$$

The errors are subjective 68.3% confidence intervals. For the SAW, we recall that Madras *et al* [20] estimated the exponent $\nu_{\rm SAW}$ using the pivot algorithm up to $N = 80\,000$. The estimate of $\nu_{\rm SAW}$ is given by (2.3) together with the following estimates of the fitting parameters:

$$A_{\rm SAW} = 0.194\,55 \pm 0.000\,07 \tag{2.9}$$

$$B' = -0.114\,32 \pm 0.004\,65 \tag{2.10}$$

$$\Delta = 0.56 \pm 0.03. \tag{2.11}$$

Here, B' corresponds to AB in our estimated values. The estimate (2.6) is in good agreement with that of the RG argument (2.2) and that of the simulation for the SAW (2.3).

From (2.7) and (2.9), we obtain the amplitude ratio

$$\frac{\langle R_{\rm G}^2 \rangle_{\rm SAP}}{\langle R_{\rm G}^2 \rangle_{\rm SAW}} = 0.566 \pm 0.019 \tag{2.12}$$

where an error is a subjective 68.3% confidence interval. The amplitude ratio (2.12) is consistent with the estimated value of the RG argument (2.1). The estimate of [19] is a

little smaller than (2.12). However, it should be consistent with the estimate of [19], if we consider the fact that the step numbers N of the simulations in [19] are much less than 30 000.

3. The characteristic length $N(\emptyset)$

3.1. A method of evaluating the knotting probability

We evaluate the knotting probability in the following way. We generate M SAPs of N steps and then enumerate the number $M(K)$ of those polygons which are equivalent to a given knot type K. We define the knotting probability $P_{\mathrm{K}}(N)$ by the ratio $M(K)/M$.

In our simulation, we determine knot types of SAPs using the second-order Vassiliev-type invariant and the Alexander polynomial evaluated at $t = -1$. The Vassiliev-type invariants have the following advantages: (1) we can calculate them in polynomial time, and (2) we can calculate them without consuming a large memory area [28]. The Vassiliev-type invariants are not complete invariants. However, in the practical sense we can safely say that if the value of the Vassiliev-type invariant computed for a SAP is zero, this SAP is a trivial knot. We will see in section 3.3 that complicated knots are very rare events in our data. Even if non-trivial knots are misidentified as the trivial knot by the Vassiliev-type invariant (this chance is very small), it would not affect the results of this paper.

For calculating the knotting probability, we generate random sequences of SAPs. We make five seeds for each of the six step numbers $N = 500$, 1000, 1500, 2000, 2500 and 3000, and then apply an operator P on them a large number of times (20 000 times). Here, P denotes 200 successful MOS pivots (see appendix A). Then, we effectively get random sequences of SAPs. A sequence of SAPs derived from each seed has a set of 20 000 SAPs. Here the sequence consists of $20\,000 \times 200$ successful MOS pivot operations. For each step number N, we thus get samples of 100 000 SAPs.

In order to analyse the behaviour of the knotting probability, we use the fitting formula (1.1). Here, we write it again:

$$P_{\mathrm{K}}(N) = C(K)N^{m(K)} \exp\left[-\frac{N}{N(K)}\right]$$

where $C(N)$, $N(K)$ and $m(K)$ are fitting parameters. In particular, $N(K)$ is called the characteristic length with knot-type K. This formula was introduced by Deguchi and Tsurusaki [12, 14, 15]. They pointed out that the formula (1.1) is suitable for the knotting probabilities of the Gaussian and rod–bead models. We will show that this is also suitable for the knotting probability $P_{\mathrm{K}}(N)$ of the cubic lattice model.

3.2. The random events of knotted polygons

Let us discuss the statistics of knotted polygons generated in our simulation. We will see in section 3.3 that almost all polygons are of trivial knots. Therefore, we may assume that non-trivial knots are generated such as the Poisson random events: the number of trivial knots between two knotted SAPs will follow the Poisson distribution, if the SAPs are randomly constructed.

Let us consider the 'time interval' of the Poisson random events. We recall that the time t is a discrete number. We measure the length L of the time interval of SAPs from time t_1 at which a knotted SAP appears, to time t_2 at which the next knotted SAP appears after t_1, and set $L = t_2 - t_1$. If non-trivial knots are generated as the Poisson random events, the time interval L follows the function

$$D(N, L) = A(N)\, P_{\emptyset}(N)^{L-1}. \tag{3.1}$$

Table 1. The number of generated knots. The estimated errors correspond to one standard deviation.

Step numbers	$M(\emptyset)$	$M(3_1)$	$M(4_1)$	etc	M
500	$99\,849 \pm 25$	147 ± 24	3 ± 3	1 ± 1	100 000
1000	$99\,640 \pm 38$	344 ± 37	9 ± 6	7 ± 5	100 000
1500	$99\,430 \pm 48$	541 ± 46	24 ± 10	5 ± 4	100 000
2000	$99\,208 \pm 56$	752 ± 55	27 ± 10	13 ± 7	100 000
2500	$98\,965 \pm 64$	985 ± 62	38 ± 12	12 ± 7	100 000
3000	$98\,787 \pm 69$	1157 ± 68	40 ± 13	16 ± 8	100 000

We call it the discrete distribution function of the time interval L. Here, $P_\emptyset(N)$ is the knotting probability for the trivial knot. We have introduced $A(N)$ for a technical reason and hence $D(N, L)$ is not necessarily normalized.

The discrete distribution functions of the time interval L are numerically evaluated as follows. The time interval L is a discrete random variable. We introduce a sequence of natural numbers $\{l_0, l_1, \ldots\}$, where $l_i = 50 \times i$. Then, we count the number of polygons with L taking values in $[l_i, l_{i+1})$ and plot it at l_i for each i. This is the discrete distribution function of the time interval L obtained from numerical evaluation.

We plot the discrete distribution functions obtained by the numerical evaluation and $D(N, L)$ as a function of L, where $P_\emptyset(N)$ is estimated from table 1 and $A(N)$ is chosen to fit these distributions (see figures 2(a) and (b)). Error bars denote one standard deviation. They are estimated by applying the Poisson distribution to the number of samples included in interval L. For $N = 1000, 1500, 2000, 2500$ and 3000, these graphs show a fairly good agreement with the function $D(N, L)$. In the case of $N = 500$, the data deviate from the function. This is not unexpected since we have too few samples of knotted polygons. We do not plot the graph for $N = 500$ in this paper.

We expect from figures 2(a) and (b) that the MOS pivot makes a uniform ensemble for knots. Thus, we can calculate the knotting probability and the characteristic length using the MOS pivot.

3.3. The number of unknotted polygons

Table 1 gives the number of each knot type with respect to N. Here, errors correspond to 68.3% confidence intervals. They are estimated by applying the binomial distribution to the number $M(K)$ of polygons for knot K. In table 1 we explain the notations: $\emptyset, 3_1, 4_1$ denote the trivial knot, the trefoil knot and the figure-eight knot, respectively. The other knot types are denoted by etc.

Table 1 shows clearly that almost all the generated SAPs are trivial knots. $M(3_1)$ is also much larger than $M(4_1)$. The other knots (etc) are nearly equal to zero.

Next we focus on the knotting probability for the trivial knot, and plot $P_\emptyset(N)$ as a function of N (figure 3). The error bars are one standard deviation. $P_\emptyset(N)$ decays linearly with respect to N. It is expected that $P_\emptyset(N)$ decays exponentially when N goes to infinity. In [1–3] it was shown that the knotting probability $P_\emptyset(N)$ tends to zero 'exponentially':

$$P_\emptyset(N) = A \exp[-\kappa N + o(N)] \qquad \text{when} \quad N \to \infty. \tag{3.2}$$

Thus, this is a natural situation.

The asymptotic shape (3.2) is realized for the trivial knot in our case when the fitting parameters of the formula (1.1) take the following values: $|m(\emptyset)| \ll 1$ and $C(\emptyset) \simeq 1$. In fact,

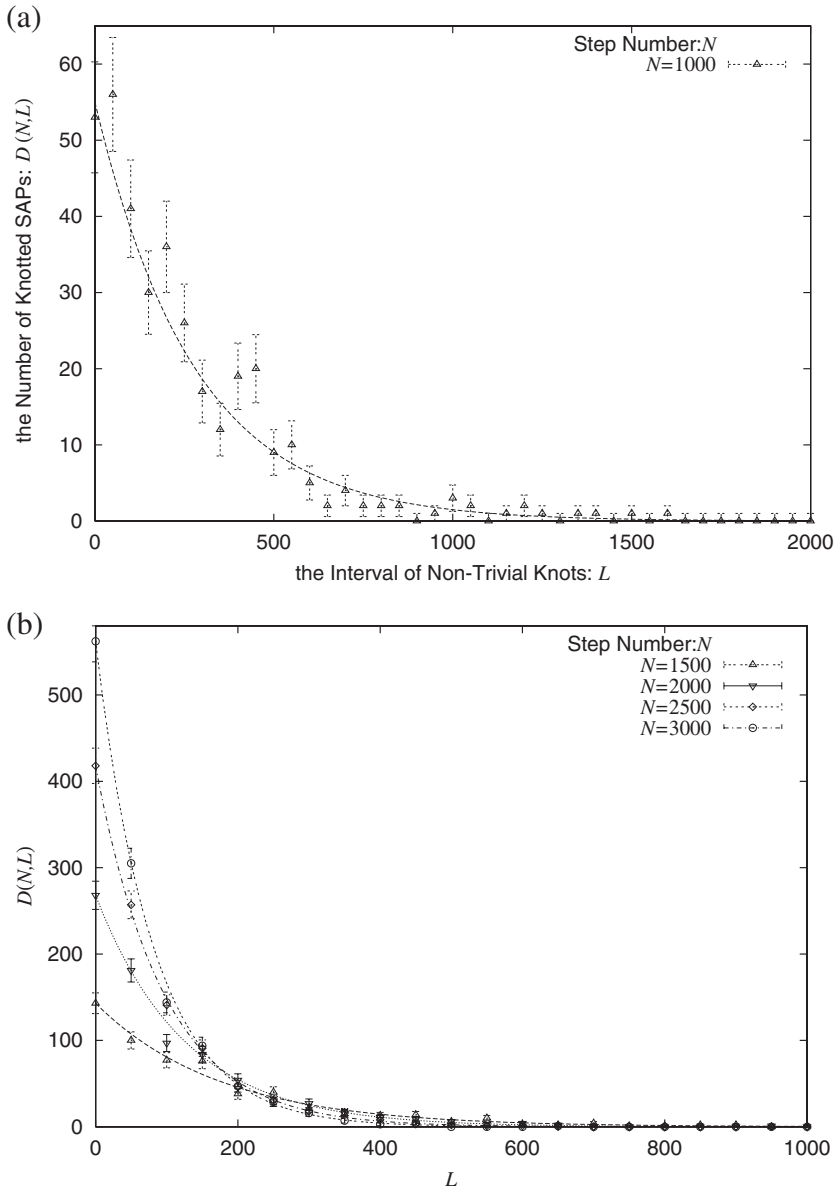

Figure 2. (*a*) Discrete distribution function of interval L of non-trivial knots for $N = 1000$. The number of knotted SAPs occurring with respect to the time interval L is represented by the Poisson distribution $D(N, L) = A(N)P_{\emptyset}(N)^L$. $P_{\emptyset}(N)$ is the knotting probability of the trivial knot with the step number N and $A(N)$ is a normalization factor. We call it the discrete distribution function of the time interval L. In our simulation, we count the number of polygons with L taking values in $[l_i, l_{i+1})$ and plot it at l_i for each subscript i. Here, the sequence $\{l_0, l_1, \ldots\}$ is defined by $l_i = 50 \times i$. The data are fitted to the distribution $D(N, L)$. We measure the length of the time interval of SAPs from time t_1 at which a knotted SAP appears to time t_2 at which the next knotted SAP appears after t_1, and denote it by L $(= t_2 - t_1)$. (*b*) Discrete distribution function of interval L of non-trivial knots for $N = 1500$, 2000, 2500 and 3000. We plot the distributions $D(N, L)$ and the data of L taking values in $[l_i, l_{i+1})$ for the step number from $N = 1500$ to 3000, respectively. The data are fitted to $D(N, L)$ well. Therefore, the MOS pivot generates SAPs without biasing statistics of knots.

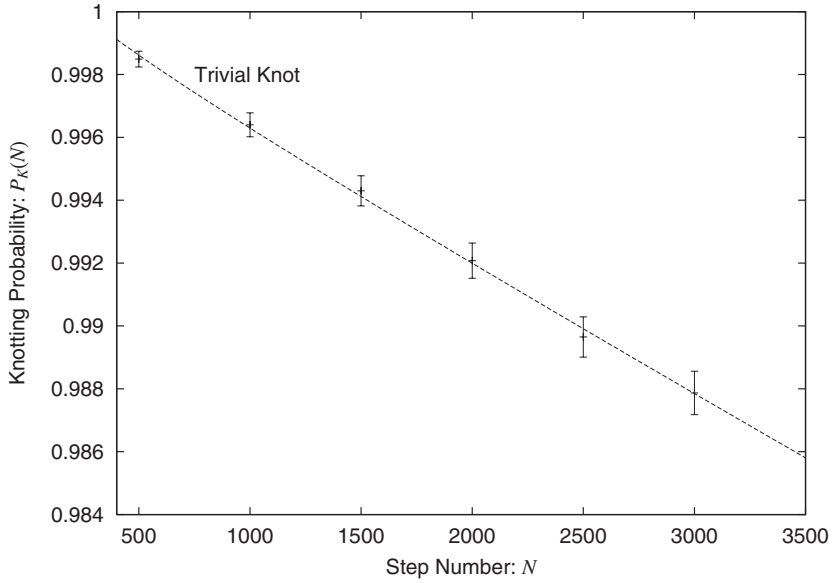

Figure 3. Knotting probability $P_{\emptyset}(N)$. We give the graph of the knotting probability $P_{\emptyset}(N)$ for the trivial knot versus the step number N. Here error bars denote one standard deviation. The data behaves as a linear decay with respect to N.

using the least-squares estimation, we find

$$C(\emptyset) = 1.0035 \pm 0.0035 \tag{3.3}$$

$$m(\emptyset) = (-4.7 \pm 5.7) \times 10^{-4} \tag{3.4}$$

$$N(\emptyset) = (2.5 \pm 0.3) \times 10^{5} \tag{3.5}$$

$$\chi^2 = 0.748 \tag{3.6}$$

$$\text{Prob}\,(\chi^2 > 0.748) = 0.862 \tag{3.7}$$

(errors are one standard deviation). Here, the χ^2 value (i.e. the sum of square of normalized deviations from the regression line) can serve as a criterion of good fit. It should be distributed as χ^2 with $n - 3$ degrees of freedom, where n is the number of data points in the fit. Prob $(\chi^2 > 0.748)$ is the probability that χ^2 would exceed the observed value, in this case 86.2%. This implies that the formula (1.1) is suitable. It is remarkable that the characteristic length of the trivial knot is much larger than the value expected from the rod–bead model.

There have been a few simulation studies on several lattices. In [11] the knotting probability for the trivial knot was calculated on a FCC lattice. It was shown that, assuming the two-parameter fitting formula, $P_{\emptyset}(N) = C(\emptyset)\mathrm{e}^{-\alpha(\emptyset)N}$, the parameters were given by

$$\alpha(\emptyset) = (7.6 \pm 0.9) \times 10^{-6}$$

$$C(\emptyset) = 1.0011 \pm 0.003$$

$$\chi^2 = 2.7$$

$$\text{Prob}\,(\chi^2 > 2.7) = 0.44$$

where errors were one standard deviation. Our interpretation of $\alpha(\emptyset)$ taking 7.6×10^{-6} is that the characteristic length is 1.3×10^{5}. Comparing the cubic lattice with the FCC lattice, the characteristic length is larger on the cubic lattice than on the FCC lattice. In [3] it was also

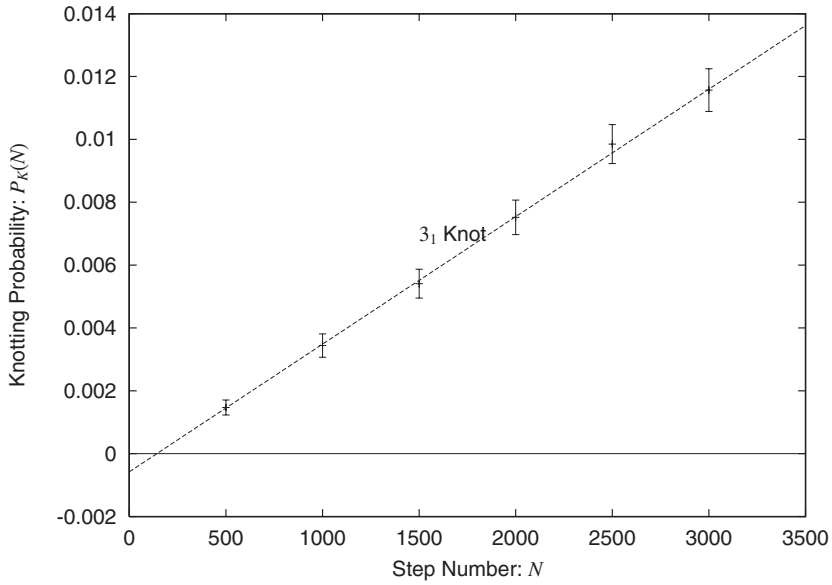

Figure 4. Knotting probability $P_{3_1}(N)$. We give the graph of the knotting probability $P_{3_1}(N)$ of trefoils versus the step number N. Here error bars denote one standard deviation. If we assume a finite-size effect for the SAPs of trefoils, we fit the data to the straight line which intersects the x-axis at a positive value.

shown that the exponent $\alpha(\emptyset)$ in the above form was $(5.7 \pm 0.5) \times 10^{-6}$ on the cubic lattice. This corresponds to the characteristic length of 1.8×10^5. We can expect that this is consistent with our estimated value within the error bars. Here we note that the connection of [16] shall be discussed in section 4 and also note that the simulation results of [29, 30] seem to contain some information on the characteristic length of the SAP on the cubic lattice. However, we are unable to derive any appropriate estimate from them.

Let us return to our data. We estimate not only the characteristic length $N(\emptyset) \simeq 2.5 \times 10^5$ but also the exponent of a correction term $m(\emptyset) \simeq 0$. These parameters show that the knotting probability for the trivial knot serves a 'pure exponential' decay on the cubic lattice. This is a new result for the cubic lattice model. Thus, the simulation in this paper improves that of [3].

We have several interpretations of the characteristic length $N(\emptyset)$. Since $N(\emptyset)$ is so large, we found that the number of knotted polygons are much smaller than that of unknotted polygons in our simulation. We expect that the knotting probability for the trivial knot decreases to about 30% at $N = N(\emptyset)$. Thus, non-trivial knots become the majority of the SAPs when N is larger than $N(\emptyset)$. In addition to this, we will see in section 4 that $N(\emptyset) \simeq N(K)$ for any knot type K is due to the fact that $N(\emptyset)$ is large.

In figure 4, we plot the knotting probability for the trefoil knot $P_{3_1}(N)$ as a function of N, where error bars are one standard deviation. The data points almost lie on a straight line. Since the data of the trefoil knot are only six points in the step number, we cannot fit the knotting probability $P_{3_1}(N)$ to formula (1.1). We leave the selection of fitting parameters for the trefoil knot or more complicated knots to future investigations.

The knotting probability $P_{3_1}(N)$ may have a finite-size effect. When we set $m(3_1) = 1$ as expected from [14, 16], the formula (1.1) does not match with $P_{3_1}(N)$ in our data. Deguchi and Tsurusaki argued that a finite-size effect appeared in the knotting probabilities in [14]. When we plot the straight line fitted to $P_{3_1}(N)$, the line intersects with the x-axis at a positive

value. This is the finite-size effect. We introduce the offset parameter $N_{\rm ini}$ and replace N by $\tilde{N} = N - N_{\rm ini}$ in the formula (1.1). When we fix $m(3_1) = 1$, our rough estimation gives $N_{\rm ini} \sim 140$ for the trefoil knot. On the other hand, we roughly estimate $N_{\rm ini} \sim 0$ for the trivial knot. We expect that such finite-size effect would also appear in the knotting probabilities for the SAPs with more complicated knot types. It could be confirmed by generating SAPs with much larger N.

In section 2.2 we calculated the gyration radius including all possible knots, and then estimated the universal amplitude ratio and the universal exponent ν. Without classifying knot types, however, we can effectively consider only trivial knots when $N < N(\emptyset)$. The universal amplitude ratio and the universal exponent are evaluated effectively for the trivial knots, although 2% of the SAPs are non-trivial knots and we neglect their influence.

4. A consequence of the large characteristic length $N(\emptyset)$

The trivial knot dominates among SAPs on the cubic lattice when N is less than 2.5×10^5. Our interpretation is that the cubic lattice so strongly possess the excluded-volume effect that it almost prevents the appearance of knotted polygons.

We have a conjecture that the appearance of a complicated knot is a rare event on the cubic lattice. According to [12, 14, 15], non-trivial knots occupy a large number of configurations of SAPs for $N \geqslant N(\emptyset)$. We believe that the above situation is also realized on the cubic lattice. If the formula (1.1) is a suitable form of the knotting probability and if the trefoil and figure-eight knots on the cubic lattice behave like those of the continuum models, the ratio $M(4_1)/M(3_1)$ for each step number N should depend only on the ratio $C(4_1)/C(3_1)$. We recall that $M(3_1) \gg M(4_1)$ for $N < 3000$ from table 1. Then, at $N \sim 2.5 \times 10^5$ almost all SAPs are expected to be 3_1 knotted polygons on the cubic lattice unlike SAPs on the continuum models.

We see that our estimated value $N(\emptyset)$ is related to the growth constant μ from the viewpoint of Orlandini *et al* [16]. The asymptotic behaviour of the number of N-step polygons c_N is given by

$$c_N = aN^{\alpha-3}\mu^N(1 + bN^{-\Delta} + \mathrm{o}(N^{-1})) \tag{4.1}$$

where α and Δ are critical exponents. For fixed knot type K, it is believed that the number $c_N(K)$ of polygons with knot K should have a similar form:

$$c_N(K) = a(K)N^{\alpha(K)-3}\mu(K)^N(1 + b(K)N^{-\Delta(K)} + \mathrm{o}(N^{-1})). \tag{4.2}$$

Then, the knotting probability $P_{\rm K}(N)$ is given by $c_N(K)/c_N$, and this implies that the characteristic length $N(\emptyset)$ relates to the growth constants μ and $\mu(\emptyset)$. We can estimate the ratio $\mu/\mu(\emptyset)$ from the value of $N(\emptyset)$:

$$\frac{\mu}{\mu(\emptyset)} \simeq \mathrm{e}^{1/N(\emptyset)} \sim 1 + (4 \pm 2) \times 10^{-6} \tag{4.3}$$

where an error is two standard deviations.

Let us discuss the independence of the characteristic length $N(K)$ with respect to knot type K. Orlandini *et al* [16] calculated the growth constants directly and showed the following equality:

$$\mu(\emptyset) = \mu(K) = 4.6836 \pm 0.0038 \qquad \text{for any knot type} \quad K \tag{4.4}$$

where an error corresponds to a 95% confidence interval. In addition Guttmann estimated the growth constant [31]

$$\mu = 4.683\,93 \pm 0.000\,02 \tag{4.5}$$

using exact enumeration and series analysis (an error is one standard deviation). From (4.4) and (4.5), we obtain the ratio

$$\frac{\mu}{\mu(\emptyset)} = \frac{\mu}{\mu(K)} \simeq 1 + (7 \pm 8) \times 10^{-5} \tag{4.6}$$

where an error is two standard deviations. From (4.3) and (4.6), we expect that the characteristic length is independent of the knot type: $N(\emptyset) \simeq N(K) \sim 2.5 \times 10^5$ for any knot type K.

Although the independence of $\mu(K)$ with respect to knot type K is pointed out by Orlandini *et al* [16], we can also confirm it more precisely through our simulation. While Orlandini *et al* [16] calculated the growth constants, we have no direct calculation for them. However, we can predict that the difference between $\mu(\emptyset)$ and $\mu(K)$ is very small when we use the following inequalities: $\liminf_{N\to\infty} N^{-1} \log c_N(K) \geqslant \mu(\emptyset)$ and $\limsup_{N\to\infty} N^{-1} \log c_N(K) < \mu$ for any knot type K, which were proven in [3, 4]. If both $\liminf_{N\to\infty} N^{-1} \log c_N(K)$ and $\limsup_{N\to\infty} N^{-1} \log c_N(K)$ exist and take the same value $\mu(K)$, then we have $\mu(\emptyset) \leqslant \mu(K) < \mu$. These inequalities and the estimate (4.3) limit the ratio $\mu(K)/\mu(\emptyset)$ to

$$\left| \frac{\mu(K)}{\mu(\emptyset)} - 1 \right| \leqslant (4 \pm 2) \times 10^{-6}. \tag{4.7}$$

This is a strong bound. Thus, we can expect that $\mu(\emptyset) \simeq \mu(K)$ for any knot type K.

Acknowledgments

We would like to thank Takeo Inami for a careful reading of the manuscript and valuable comments. AY is supported by a Research Assistant Fellowship of Chuo University. This work is partially supported by the Grant-in-Aid for Encouragement of Young Scientists (No 12740231).

Appendix A. The method for generating SAPs

Let us discuss the method for making SAPs employed in this paper. We first construct a seed SAP w, and then derive a random sequence of SAPs $\{w^{[1]}, w^{[2]}, \ldots, w^{[t-1]}, w^{[t]}, \ldots\}$, where $w^{[t]} = P(w^{[t-1]})$ and $w^{[0]} = w(0)$. Here the operator P will be defined later.

We construct a 'seed' SAP, by combining two SAWs which have the same endpoints, in the following way: first we make an $N/2$-step SAW using the myopic self-avoiding walk (MSAW) algorithm [32], where N is an even integer; secondly we perform the MOS pivot transformations with respect to $k = 0, l = N/2$ [21]; finally we concatenate the endpoints of the new and original SAWs respectively (figure A.1), and get an SAP with the step number N if it has no self-intersections.

Let us discuss how to construct a random sequence of SAPs in our simulations. If one of the MOS pivot transformations changes a given SAP into a different SAP, this operation is called a successful MOS pivot operation. We consider a sequence of successful MOS pivot operations. Then, we define an operator P by 200 successful MOS pivot operations in the sequence. We note that the SAP obtained by a single successful MOS pivot is not independent from the original one: they are correlated. However, the correlation decays almost completely after 200 successful MOS pivot operations, which shall be shown in appendix B. Thus, we may consider that for any given SAP w, $P(w)$ is independent from w.

For generating SAPs, we use the Mersenne twister which is a pseudo-random number generator [33]. This algorithm has the following properties: (1) we can get many samples because the period is $2^{19\,937} - 1$, (2) we treat high-dimensional space (max 623 dimensions),

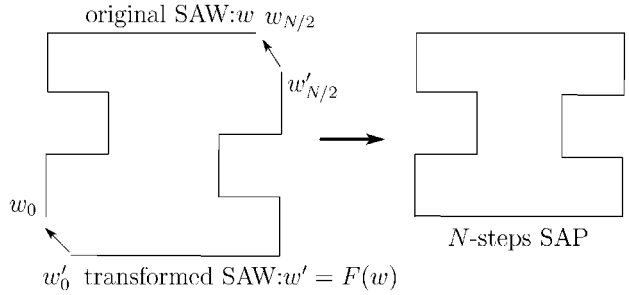

Figure A.1. Generated seed SAP with step number N. An original SAW w generated by the MSAW algorithm with the step number $N/2$ transforms into another SAW using the MOS pivot with respect to $k = 0$ and $l = N/2$. We concatenate the edges of new and original SAWs, respectively. We get an N-step SAP.

(3) pseudo-random numbers are generated quickly and (4) we can use the memory efficiently. Thus, the Mersenne twister is a high-performance generator.

Appendix B. The decay of correlations between the SAPs obtained by the MOS pivot operations

In order to check the validity of the random sequence of SAPs constructed in this paper, we show explicitly how the correlation between the SAPs decays after applying a number of MOS pivot operations.

Let us regard the number τ of successful MOS pivot operations as the time of evolution of the SAP shape under the sequential MOS pivot operations: the seed SAP w of a random sequence corresponds to $w(0)$ for $\tau = 0$; $w(\tau)$ is defined by $p^{\tau}(w)$ for $\tau > 0$. Here p denotes a successful MOS pivot operation. Let us now define the correlation function for the SAP structure with the step number N in the following

$$C(\tau) = \frac{\sum_{\alpha=1}^{3}\sum_{i=0}^{N-1}\langle (w_i^{(\alpha)}(0) - \frac{1}{N}\sum_{j=0}^{N-1} w_j^{(\alpha)}(0))(w_i^{(\alpha)}(\tau) - \frac{1}{N}\sum_{l=0}^{N-1} w_l^{(\alpha)}(\tau))\rangle}{\sum_{\alpha=1}^{3}\sum_{i=0}^{N-1}\langle (w_i^{(\alpha)}(0) - \frac{1}{N}\sum_{j=0}^{N-1} w_j^{(\alpha)}(0))^2\rangle} \tag{B.1}$$

where $w_i^{(\alpha)}(\tau)$ is the α-component of the ith site of the SAP (or SAW) after τ pivot operations and $\langle\cdot\rangle$ denotes the statistical average.

In figures B.2(a) and (b), we plot the correlation $C(\tau)$ versus time τ in the cases of $N = 500$ and 1000, respectively. Error bars show one standard deviation which are estimated by assuming that the data follows the Poisson distribution. In our simulation, we evaluated the correlations of SAPs with the step number N at 500 and 1000, and generated 10 000 sequences (starting from 10 000 different seeds) to take the statistical average.

The decay rate of the correlation function $C(\tau)$ is slower in the case of the MOS pivot than in the case of the normal pivot algorithm (figures B.2(a) and (b)). This is due to the difference in the numbers of independent pivot transformations. Note that the number of independent transformations for the normal pivot algorithm [20, 32] is $d!2^d - 1$ (the normal pivot algorithm is an algorithm with one endpoint free while the other fixed), which correspond to the number of all the elements of the d-dimensional orthogonal group on a hypercubic lattice, while for the MOS pivot $2d(d-1)+1$ in the d-dimensional hypercubic lattice. In the cubic lattice, the MOS pivot has 13 pivot transformations while the normal pivot algorithm has 47.

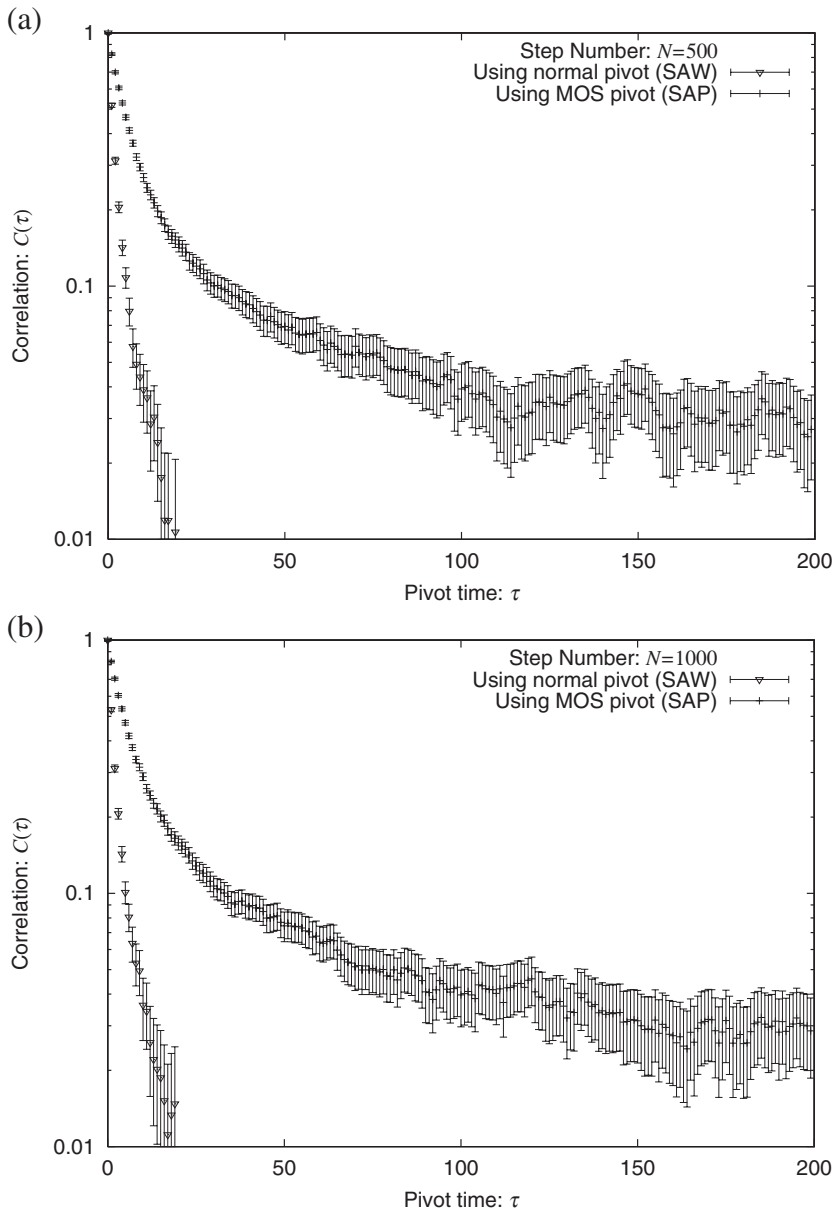

Figure B.2. (*a*) Pivot correlation $C(\tau)$ at $N = 500$. We plot the pivot correlations $C(\tau)$ versus time τ. The MOS pivot and the normal pivot operations in the case of $N = 500$, respectively. Here, τ is the number of trials, and error bars correspond to one standard deviation. The correlation of the MOS pivot decays slower than that of the normal pivot. (*b*) Pivot correlation $C(\tau)$ at $N = 1000$. Similarly to (*a*) we plot the pivot correlations $C(\tau)$ versus time τ. The MOS pivot and the normal pivot operations in the case of $N = 1000$, respectively. Here, τ is the number of trials, and error bars correspond to one standard deviation. At $\tau = 200$, we consider correlations $C(\tau)$ as zero focusing on the MOS pivot correlations for $N = 500$ and 1000.

References

[1] Sumners D W and Whittington S G 1988 *J. Phys. A: Math. Gen.* **21** 1689
[2] Pippenger N 1989 *Discrete Appl. Lett. Math.* **25** 273
[3] Whittington S G 1992 *AMS Proc. Symp. Appl. Math.* **45** 73
[4] Soteros C E, Sumners D W and Whittington S G 1992 *Math. Proc. Camb. Phil. Soc.* **111** 75
[5] Vologodskii A V, Lukashin A V, Frank-Kamenetskii M D and Anshelevich V V 1974 *Sov. Phys.–JETP* **39** 1059
[6] Michels J P J and Wiegel F W 1982 *Phys. Lett.* A **90** 381
[7] Le Bret M 1980 *Biopolymers* **19** 619
[8] Chen Y D 1981 *J. Chem. Phys.* **74** 2034
Chen Y D 1981 *J. Chem. Phys.* **75** 2447
Chen Y D 1981 *J. Chem. Phys.* **75** 5160
[9] Klenin K V, Vologodskii A V, Anshelevich V V, Dykhne A M and Frank-Kamenetskii M D 1988 *J. Biomol. Struct. Dyn.* **5** 1173
[10] Koniaris K and Muthukumar M 1991 *Phys. Rev. Lett.* **66** 2211
[11] Janse van Rensburg E J and Whittington S G 1990 *J. Phys. A: Math. Gen.* **23** 3573
[12] Deguchi T and Tsurusaki K 1994 *J. Knot Theory and Its Ramifications* **3** 321
[13] Deguchi T and Tsurusaki K 1997 *Geometry and Physics (Lecture Notes in Pure and Applied Mathematics Series vol 184)* ed J E Andersen, J Dupont, H Pedersen and A Swann (Basel: Marcel Dekker) pp 557–65
Deguchi T and Tsurusaki K 1995 *Proc. Geometry and Physics (Institute of Mathematics, University of Aarhus, Aarhus, Denmark, July 1995)*
[14] Deguchi T and Tsurusaki K 1997 *Phys. Rev.* E **55** 6245
[15] Deguchi T and Tsurusaki K 1997 *Lectures at Knots96* (Singapore: World Scientific) p 95
[16] Orlandini E, Tesi M C, Janse van Rensburg E J and Whittington S G 1998 *J. Phys. A: Math. Gen.* **31** 5953
[17] Delbrück M 1962 *Proc. Symp. Appl. Math.* **4** 55
[18] des Cloizeaux J and Mehta M L 1979 *J. Physique (Paris)* **40** 665
[19] Tesi M C, Janse van Rensburg E J, Orlandini E and Whittington S G 1996 *J. Phys. A: Math. Gen.* **29** 2451
[20] Li B, Madras N and Sokal A D 1995 *J. Stat. Phys.* **80** 661
[21] Madras N, Orlitsky A and Shepp L A 1990 *J. Stat. Phys.* **58** 159
[22] Prentis J J 1982 *J. Chem. Phys.* **76** 1574
[23] Lipkin M, Oono Y and Freed K F 1981 *Macromolecules* **14** 1270
[24] LeGuillou J C and Zinn-Justin J 1980 *Phys. Rev.* B **21** 3976
[25] LeGuillou J C and Zinn-Justin J 1985 *J. Phys. Lett.* **46** L-137
[26] LeGuillou J C and Zinn-Justin J 1989 *J. Physique (Paris)* **50** 1365
[27] Guida R and Zinn-Justin J 1997 *Preprint* SPhT-t97/040
[28] Deguchi T and Tsurusaki K 1993 *Phys. Lett.* A **174** 29
[29] Janse van Rensburg E J and Whittington S G 1991 *J. Phys. A: Math. Gen.* **24** 3953
[30] Orlandini E, Tesi M C, Janse van Rensburg E J and Whittington S G 1996 *J. Phys. A: Math. Gen.* **29** L299
[31] Guttmann A J 1989 *J. Phys. A: Math. Gen.* **22** 2807
[32] Madras N and Slade G 1993 *The Self-Avoiding Walk* (Basle: Birkhäuser)
[33] http://www.math.keio.ac.jp/ matumoto/emt.html